Current Integral Comparison-Based Power Loss Balancing Control for Full-Bridge Modular Multilevel Converters

Huailong Li, Fujin Deng, *Senior Member, IEEE*, Jie Tian, Yu Lu, Gang Li, and Frede Blaabjerg, *Fellow, IEEE*

***Abstract*—Power loss management is one of the most important challenges for improving the reliability of modular multilevel converters (MMCs). This article proposes a current integral comparison (CIC)-based power loss balancing control (PLBC) for full-bridge submodule (FBSM)-based MMCs, where two types of bypassed modes of the FBSM are selected by comparing the current difference integral values of the semiconductors in the FBSM. The proposed control can not only improve the power loss distribution in each FBSM, but also reduce the temperature fluctuation of semiconductors, and accordingly, the proposed control significantly improves the lifetime of MMCs. Simulation studies with professional tool PSCAD/EMTDC and experimental studies with a downscale MMC prototype are conducted, and their results confirm the effectiveness of the proposed CIC-PLBC.**

***Index Terms*—Full-bridge submodule (FBSM), modular multilevel converter (MMC), power loss, reliability, temperature fluctuation.**

I. Introduction

MODULAR multilevel converters (MMCs) have become increasingly attractive for medium-/high-voltage and high-power applications owing to the advantages of modular design, low switching frequency, and low harmonics [1], [2], [3], [4]. The full-bridge submodule (FBSM)-based MMC is much preferred in high-voltage direct-current (HVdc) applications, since it offers an invaluable feature of dc fault current limiting [5], [6], [7]. In addition, the negative voltage state of FBSM can be utilized to boost the ac voltage and decrease SM capacitor ripples [8].

Power loss distribution among the semiconductors in each SM is normally unbalanced [9], due to the dc components in the arm currents and asymmetric switching signals of the semiconductors, which will affect the overall reliability of the MMC. Therefore, it is vital to improve the power loss distribution among semiconductors in each SM.

So far, several methods have been presented to balance the power losses among semiconductors, which can be divided into SM design-based method, control strategy-based method, and modulation optimization-based method. SM design-based method can improve the power loss distribution in each SM. Hohmann and Bakran [10] presented a half-bridge (HB) SM topology with an additional antiparallel diode, which can reduce the power loss of bottom diode. Li et al. [11] presented an HBSM topology with a bypass thyristor, which can reduce the power loss differences between the top and bottom IGBT/diode in each HBSM. However, the SM design-based method would complicate the hardware design.

Control strategy-based method also plays an important role in balancing the power loss distribution in each SM. Merlin and Mitcheson [12] presented an active power loss distribution control for HBSMs based on an added dc voltage offset in the converter voltage waveform. Zhao et al. [13] presented an optimum circulating current injection control, which can reduce the maximum power loss in each HBSM. Qiu et al. [14] presented a device-level loss balancing control, which can balance the power losses in HBSMs through regulating the capacitor voltages. However, all above methods only focus on balancing power losses in the HBSMs.

Modulation optimization-based method is another solution to regulate power losses among semiconductors in each FBSM. Sheng et al. [15] presented a rotation bypassed mode (BM) modulation to improve the power loss distribution. However, the power losses among the semiconductors are still unbalanced. Li et al. [16] presented an improved phase-shifted carrier-based modulation for FBSMs, where two types of BMs are selected in rotation. However, the control in [16] cannot eliminate the power loss differences and would cause severe temperature fluctuation of semiconductors, which would deteriorate the MMC reliability.

In this article, the power loss distribution among semiconductors in the FBSM under various switching modes is analyzed in details. A current integral comparison-based power loss balancing control (CIC-PLBC) is proposed to balance the power losses in the FBSM, where two types of BMs are selected by comparing

Manuscript received 2 April 2023; revised 14 July 2023; accepted 20 August 2023. Date of publication 4 September 2023; date of current version 23 October 2023. This work was supported by the Science and Technology Projects of Jiangsu Province under Project BE2022016. Recommended for publication by Associate Editor D. Dong. *(Corresponding author: Fujin Deng.)*

Huailong Li is with the School of Electrical Engineering, Southeast University, Nanjing 210096, China (e-mail: 230218875@seu.edu.cn).

Fujin Deng is with the School of Electrical Engineering, Jiangsu Key Laboratory of Smart Grid Technology and Equipment, Southeast University, Nanjing 210096, China (e-mail: fdeng@seu.edu.cn).

Jie Tian, Yu Lu, and Gang Li are with the NR Electric Company, Ltd., Nanjing 211102, China (e-mail: tianj@nrec.com; luy@nrec.com; ligang@nrec.com).

Frede Blaabjerg is with the Department of Energy Technology, Aalborg University, 9220 Aalborg, Denmark (e-mail: fbl@et.aau.dk).

Color versions of one or more figures in this article are available at https://doi.org/10.1109/TPEL.2023.3311402.

Digital Object Identifier 10.1109/TPEL.2023.3311402

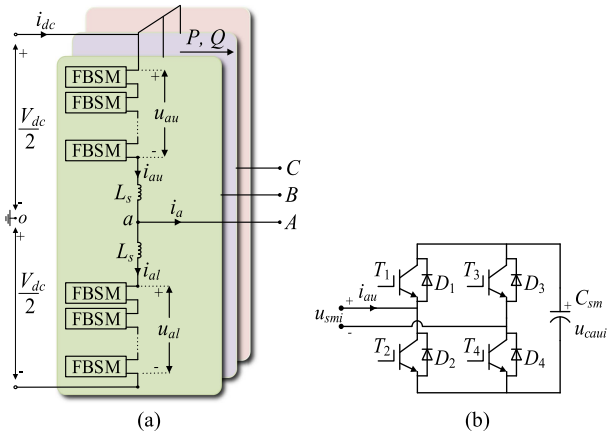

Fig. 1. (a) Three-phase MMC. (b) FBSM unit.

TABLE I
OPERATION OF FBSMS

S_i	u_{smi}	Mode	T_1	T_2	T_3	T_4
1	u_{caui}	1	ON	OFF	OFF	ON
-1	$-u_{caui}$	-1	OFF	ON	ON	OFF
0	0	0A	OFF	ON	OFF	ON
		0B	ON	OFF	ON	OFF

the current difference integral values of semiconductors in the FBSM. The primary contributions of this article are as follows:

1) it reveals that the power loss distribution in FBSMs is unbalanced with traditional rotation BM method;
2) it reveals that the temperature fluctuation of semiconductors is severe with traditional rotation BM method;
3) it balances the power loss distribution and reduces the temperature fluctuation of semiconductors in FBSMs;
4) it significantly improves the lifetime of MMCs.

The rest of this article is organized as follows. Section II demonstrates the operation of the FBSM-based MMC. Sections III and IV analyze the power loss distribution in the FBSM. Section V proposes the CIC-PLBC for the FBSM-based MMC. System simulation and experimental tests are presented in Sections VI and VII, respectively, to verify the effectiveness of the proposed control. Finally, Section VIII concludes this article.

II. Operation Principle of MMCs

A. MMC Structure

A three-phase MMC is shown in Fig. 1(a). Each phase of the MMC consists of two arms and each arm comprises N identical SMs and an inductor L_s. Fig. 1(b) shows the ith SM in the upper arm of phase A, which is an FB structure and made up of a storage capacitor C_{sm} and four switches/diodes T_1/D_1–T_4/D_4 [17]. The ith FBSM's output voltage u_{smi} is

$$u_{smi} = S_i \cdot u_{caui} \tag{1}$$

where u_{caui} is the capacitor voltage and S_i is switching function, as given in Table I. When $S_i = 1$, $u_{smi} = u_{caui}$, and the FBSM works in Mode 1, where the T_1 and T_4 are switched ON and T_2 and T_3 are switched OFF. When $S_i = -1$, $u_{smi} = -u_{caui}$, and the FBSM works in Mode -1, where the T_2 and T_3 are switched ON and T_1 and T_4 are switched OFF. When $S_i = 0$, the FBSM works in one of the following two types of BMs, as follows.

1) *Mode 0A:* T_2 and T_4 are switched ON and T_1, T_3 are switched OFF, and accordingly $u_{smi} = 0$.
2) *Mode 0B:* T_1 and T_3 are switched ON and T_2, T_4 are switched OFF, and accordingly $u_{smi} = 0$.

TABLE II
RELATIONSHIP BETWEEN $I_{Tj}(I_{Dj})$ AND $P_{con\_Tj}(P_{con\_Dj})$

I_{Tj} (I_{Dj})	P_{con_Tj} (P_{con_Dj})
↑	↑
↓	↓

B. SM Conduction Loss

The conduction losses P_{con_T1}–P_{con_T4} corresponding to T_1–T_4, respectively, and the conduction losses P_{con_D1}–P_{con_D4} corresponding to D_1–D_4, respectively, are [15], [18]

$$\begin{cases} P_{\mathrm{con}\_Tj} = \frac{V_{T\mathrm{con}}}{T_f} I_{Tj} \\ P_{\mathrm{con}\_Dj} = \frac{V_{D\mathrm{con}}}{T_f} I_{Dj} \end{cases} j = 1, 2, 3, 4 \tag{2}$$

with

$$\begin{cases} I_{Tj} = \int_0^{T_f} i_{Tj} dt \\ I_{Dj} = \int_0^{T_f} i_{Dj} dt \end{cases} \tag{3}$$

where $V_{T\mathrm{con}}$ and $V_{D\mathrm{con}}$ are the drop voltages on switch and diode, respectively. T_f is the fundamental cycle and $T_f = 2\pi/\omega_0$. I_{Tj} and I_{Dj} are the integrals of the currents i_{Tj} and i_{Dj} during one fundamental period T_f, respectively. The P_{con_Tj} (P_{con_Dj}) of T_j (D_j) is proportional to I_{Tj} (I_{Dj}), which increases along with the increase of I_{Tj} (I_{Dj}) and vice versa, as given in Table II.

C. SM Switching Loss

The switching losses P_{sw_T1}–P_{sw_T4} corresponding to T_1–T_4, respectively, and the switching losses P_{sw_D1}–P_{sw_D4} corresponding to D_1–D_4, respectively, are [18]

$$\begin{cases} P_{\mathrm{sw}\_Tj} = \frac{1}{T_f} \sum_0^{T_f} \left[E_{\mathrm{on}\_Tj}(i_{Tj}) + E_{\mathrm{off}\_Tj}(i_{Tj}) \right] \\ P_{\mathrm{sw}\_Dj} = \frac{1}{T_f} \sum_0^{T_f} E_{\mathrm{rec}\_Dj}(i_{Dj}) \end{cases} \tag{4}$$

where E_{on_Tj} and E_{off_Tj} are the turn-ON energy and turn-OFF energy of the switch, respectively. E_{rec_Dj} is the reverse-recovery energy of the diode.

D. SM Total Power Loss

The total power losses P_{Loss_Tj} and P_{Loss_Dj} of the switch T_j and diode D_j, respectively, are

$$\begin{cases} P_{\mathrm{Loss}\_Tj} = P_{\mathrm{con}\_Tj} + P_{\mathrm{sw}\_Tj} \\ P_{\mathrm{Loss}\_Dj} = P_{\mathrm{con}\_Dj} + P_{\mathrm{sw}\_Dj}. \end{cases} \tag{5}$$

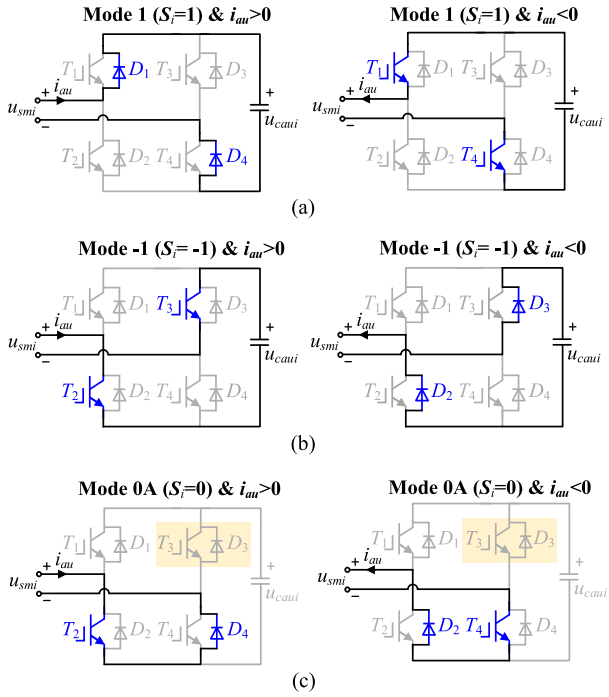

Fig. 2. Conduction situation with only Mode 0A-based BM. (a) Mode 1 ($S_i = 1$). (b) Mode -1 ($S_i = -1$). (c) Mode 0A ($S_i = 0$).

III. Power Loss Analysis of FBSM Working With Only Mode 0A-Based BM

With only Mode 0A-based BM, when $S_i = 1$, the FBSM works in Mode 1; when $S_i = -1$, the FBSM works in Mode -1; when $S_i = 0$, the FBSM works in Mode 0A, as shown in Fig. 2, as follows.

1) *Mode 1 ($S_i = 1$), as shown in* Fig. 2(a)*:* When $i_{au} > 0$, the i_{au} flows through D_1 and D_4, and the D_1's current is $i_{D1} = i_{au}$ and D_4's current is $i_{D4} = i_{au}$. When $i_{au} < 0$, the i_{au} flows through T_1 and T_4, and $i_{T1} = i_{T4} = -i_{au}$.
2) *Mode -1 ($S_i = -1$), as shown in* Fig. 2(b)*:* When $i_{au} > 0$, the i_{au} flows through T_2 and T_3, and $i_{T2} = i_{T3} = i_{au}$. When $i_{au} < 0$, the i_{au} flows through D_2 and D_3, and $i_{D2} = i_{D3} = -i_{au}$.
3) *Mode 0A ($S_i = 0$), as shown in* Fig. 2(c)*:* When $i_{au} > 0$, the i_{au} flows through T_2 and D_4, and $i_{T2} = i_{D4} = i_{au}$. When $i_{au} < 0$, the i_{au} flows through T_4 and D_2, and $i_{T4} = i_{D2} = -i_{au}$.

A. Power Losses Analysis of T_1 and T_4

Based on Fig. 2, when the FBSM works with only Mode 0A-based BM, the currents flowing through T_1 and T_4 are

$$i_{T1} = \begin{cases} -i_{au} & S_i = 1 \text{ and } i_{au} < 0 \\ 0 & \text{other situations} \end{cases} \tag{6}$$

$$i_{T4} = \begin{cases} -i_{au} & S_i = 1 \text{ and } i_{au} < 0 \\ -i_{au} & S_i = 0 \text{ and } i_{au} < 0 \\ 0 & \text{other situations.} \end{cases} \tag{7}$$

TABLE III
Power Losses With Only Mode 0A-Based BM

Semiconductor	Current integral	Conduction loss
T_1 and T_4	I_{T1}<I_{T4}	$P_{\text{con\_}T1}$<$P_{\text{con\_}T4}$
D_1 and D_4	I_{D1}<I_{D4}	$P_{\text{con\_}D1}$<$P_{\text{con\_}D4}$
T_2 and T_3	I_{T3}<I_{T2}	$P_{\text{con\_}T3}$<$P_{\text{con\_}T2}$
D_2 and D_3	I_{D3}<I_{D2}	$P_{\text{con\_}D3}$<$P_{\text{con\_}D2}$

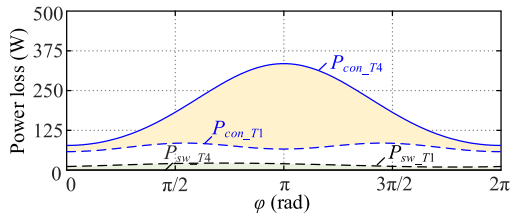

Fig. 3. Conduction losses and switching losses of T_1 and T_4 under various φ.

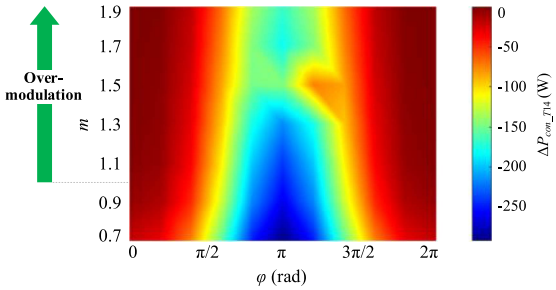

Fig. 4. Conduction loss difference $\Delta P_{\text{con\_}T14}$ under various φ and various m.

It can be observed that T_1 takes less current in comparison with T_4, and therefore, the current integral of T_1 is smaller than that of T_4 as $I_{T1} < I_{T4}$, which causes that the conduction loss of T_1 is smaller than that of T_4 as $P_{\text{con\_}T1} < P_{\text{con\_}T4}$, as given in Table III. Fig. 3 shows the conduction losses and switching losses of T_1 and T_4 in the FBSM of MMC working at the rated apparent power listed in Table VI and various power factor angles φ, which is derived from the simulation system in Section VI. In Fig. 3, the modulation index $m = 0.8$. The Infineon IGBT module FZ1200R17HP4 is adopted. The power losses are calculated based on (2)–(4) and the semiconductor specifications are provided by the datasheet [19]. It also shows that $P_{\text{con\_}T1} < P_{\text{con\_}T4}$. In addition, compared with conduction losses, the switching losses of T_1 and T_4 have little effect on power loss unbalancing due to low switching frequency of MMC with numerous SMs, as shown in Fig. 3.

Fig. 4 shows the conduction loss difference $\Delta P_{\text{con\_}T14}$ between T_1 and T_4 under various φ and various m, which is derived from the simulation system in Section VI. In Fig. 4, the MMC working with overmodulation as $m > 1$ is also considered and $\Delta P_{\text{con\_}T14} = P_{\text{con\_}T1}$-$P_{\text{con\_}T4}$. It can be observed that the $\Delta P_{\text{con\_}T14}$ is rated to φ and m, and $\Delta P_{\text{con\_}T14} < 0$ when FBSM works with only Mode 0A-based BM, which also indicates that $P_{\text{con\_}T1} < P_{\text{con\_}T4}$.

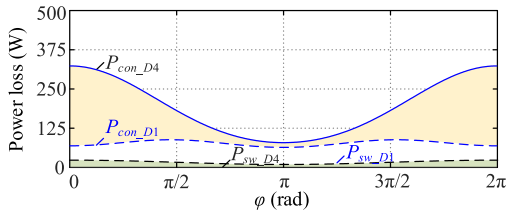

Fig. 5. Conduction losses and switching losses of D_1 and D_4 under various φ.

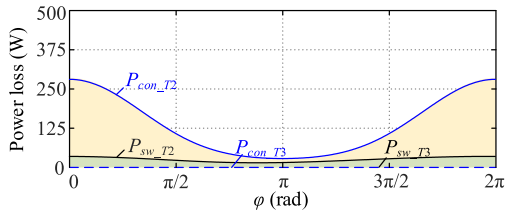

Fig. 7. Conduction losses and switching losses of T_2 and T_3 under various φ.

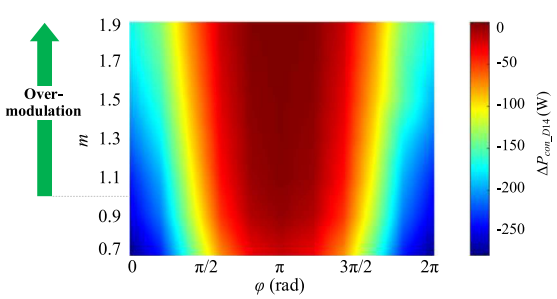

Fig. 6. Conduction loss difference $\Delta P_{\mathrm{con\_}D14}$ under various φ and various m.

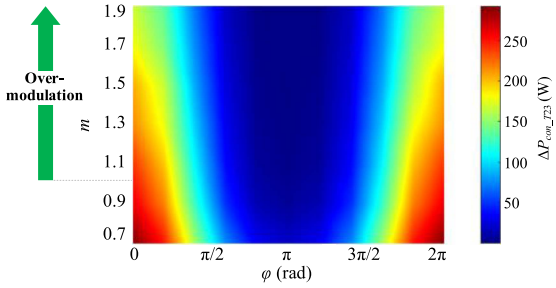

Fig. 8. Conduction loss difference $\Delta P_{\mathrm{con\_}T23}$ under various φ and various m.

B. Power Losses Analysis of D_1 and D_4

Based on Fig. 2, when the FBSM works with only Mode 0A-based BM, the currents flowing through D_1 and D_4 are

$$i_{D1} = \begin{cases} i_{au} & S_i = 1 \text{ and } i_{au} > 0 \\ 0 & \text{other situations} \end{cases} \tag{8}$$

$$i_{D4} = \begin{cases} i_{au} & S_i = 1 \text{ and } i_{au} > 0 \\ i_{au} & S_i = 0 \text{ and } i_{au} > 0 \\ 0 & \text{other situations.} \end{cases} \tag{9}$$

It can be observed that the D_1 takes less current in comparison with D_4, and therefore, the current integral of D_1 is smaller than that of D_4 as $I_{D1} < I_{D4}$, which causes that the conduction loss of D_1 is smaller than that of D_4 as $P_{\mathrm{con\_}D1} < P_{\mathrm{con\_}D4}$, as given in Table III. Fig. 5 shows the conduction losses and switching losses of D_1 and D_4 under various φ and $m = 0.8$. Fig. 6 shows the conduction loss difference $\Delta P_{\mathrm{con\_}D14} = P_{\mathrm{con\_}D1}$-$P_{\mathrm{con\_}D4}$ under various φ and various m. Figs. 4 and 5 show that the $P_{\mathrm{con\_}D1} < P_{\mathrm{con\_}D4}$ when FBSM works with only Mode 0A-based BM and the switching losses have little effect on power loss unbalancing.

C. Power Losses Analysis of T_2 and T_3

Based on Fig. 2, when the FBSM works with only Mode 0A-based BM, the currents flowing through T_2 and T_3 are:

$$i_{T2} = \begin{cases} i_{au} & S_i = -1 \text{ and } i_{au} > 0 \\ i_{au} & S_i = 0 \text{ and } i_{au} > 0 \\ 0 & \text{other situations} \end{cases} \tag{10}$$

$$i_{T3} = \begin{cases} i_{au} & S_i = -1 \text{ and } i_{au} > 0 \\ 0 & \text{other situations.} \end{cases} \tag{11}$$

It can be observed that T_3 takes less current in comparison with T_2, and therefore, the current integral of T_3 is smaller than that of T_2 as $I_{T3} < I_{T2}$, which causes that the conduction loss of T_3 is smaller than that of T_2 as $P_{\mathrm{con\_}T3} < P_{\mathrm{con\_}T2}$, as given in Table III. Fig. 7 shows the conduction losses and switching losses of T_2 and T_3 under various φ and $m = 0.8$. Fig. 8 shows the conduction loss difference $\Delta P_{\mathrm{con\_}T23} = P_{\mathrm{con\_}T2}$-$P_{\mathrm{con\_}T3}$ under various φ and various m. Figs. 7 and 8 show that the $P_{\mathrm{con\_}T3} < P_{\mathrm{con\_}T2}$ when FBSM works with only Mode 0A-based BM and the switching losses have little effect on power loss unbalancing.

D. Power Losses Analysis of D_2 and D_3

Based on Fig. 2, when the FBSM works with only Mode 0A-based BM, the currents flowing through D_2 and D_3 are

$$i_{D2} = \begin{cases} -i_{au} & S_i = -1 \text{ and } i_{au} < 0 \\ -i_{au} & S_i = 0 \text{ and } i_{au} < 0 \\ 0 & \text{other situations} \end{cases} \tag{12}$$

$$i_{D3} = \begin{cases} -i_{au} & S_i = -1 \text{ and } i_{au} < 0 \\ 0 & \text{other situations.} \end{cases} \tag{13}$$

It can be observed that D_3 takes less current in comparison with D_2, and therefore, the current integral of D_3 is smaller than that of D_2 as $I_{D3} < I_{D2}$, which causes that the conduction loss of D_3 is smaller than that of D_2 as $P_{\mathrm{con\_}D3} < P_{\mathrm{con\_}D2}$, as given in Table III. Fig. 9 shows the conduction losses and switching losses of D_2 and D_3 under various φ and $m = 0.8$. Fig. 10 shows the conduction loss difference $\Delta P_{\mathrm{con\_}D23} = P_{\mathrm{con\_}D2}$-$P_{\mathrm{con\_}D3}$ under various φ and various m. Figs. 9 and 10 show that the $P_{\mathrm{con\_}D3} < P_{\mathrm{con\_}D2}$ when FBSM works with only Mode 0A-based BM and the switching losses have little effect on power loss unbalancing.

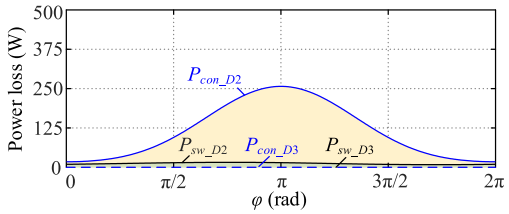

Fig. 9. Conduction losses and switching losses of D_2 and D_3 under various φ.

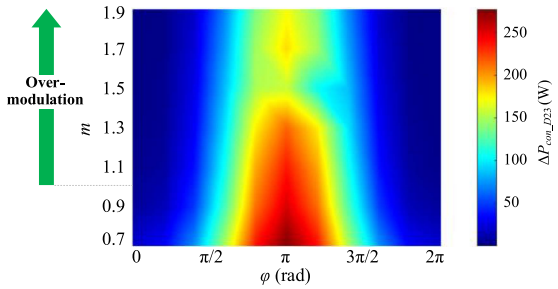

Fig. 10. Conduction loss difference $\Delta P_{\mathrm{con}\_D23}$ under various φ and various m.

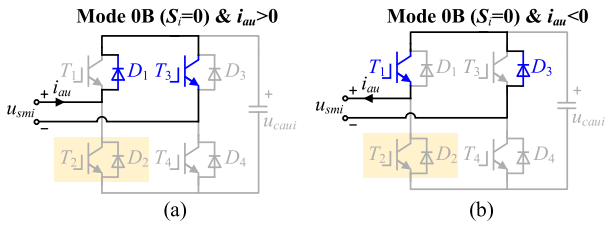

Fig. 11. Conduction situation in FBSM with mode 0B. (a) $i_{au} > 0$. (b) $i_{au} < 0$.

IV. Power Loss Analysis of FBSM Working With Only Mode 0B-Based BM

With only Mode 0B-based BM, when $S_i = 1$, the FBSM works in Mode 1; when $S_i = -1$, the FBSM works in Mode -1; when $S_i = 0$, the FBSM works in Mode 0B. The conduction situation in FBSM with Mode 0B is shown in Fig. 11, as follows.

1) *$i_{au} > 0$, as shown in* Fig. 11(a)*:* The i_{au} flows through T_3 and D_1, and the T_3's current is $i_{T3} = i_{au}$ and D_1's current is $i_{D1} = i_{au}$.
2) *$i_{au} < 0$, as shown in* Fig. 11(b)*:* The i_{au} flows through T_1 and D_3, and the T_1's current is $i_{T1} = -i_{au}$ and D_3's current is $i_{D3} = -i_{au}$.

Similar to the analysis in Section III, the power loss distribution in the FBSM with only Mode 0B-based BM is given in Table IV, as follows.

1) *T_1 and T_4:* The T_1 takes more current in comparison with T_4, and $I_{T1} > I_{T4}$, which causes $P_{\mathrm{con}\_T1} > P_{\mathrm{con}\_T4}$ according to (2).
2) *D_1 and D_4:* The D_1 takes more current in comparison with D_4, and $I_{D1} > I_{D4}$, which causes $P_{\mathrm{con}\_D1} > P_{\mathrm{con}\_D4}$ according to (2).
3) *T_2 and T_3:* The T_3 takes more current in comparison with T_3, and $I_{T3} > I_{T2}$, which causes $P_{\mathrm{con}\_T3} > P_{\mathrm{con}\_T2}$ according to (2).

TABLE IV
Power Losses With Only Mode 0B-Based BM

Semiconductor	Current integral	Conduction loss
T_1 and T_4	$I_{T1}>I_{T4}$	$P_{\mathrm{con}\_T1}>P_{\mathrm{con}\_T4}$
D_1 and D_4	$I_{D1}>I_{D4}$	$P_{\mathrm{con}\_D1}>P_{\mathrm{con}\_D4}$
T_2 and T_3	$I_{T3}>I_{T2}$	$P_{\mathrm{con}\_T3}>P_{\mathrm{con}\_T2}$
D_2 and D_3	$I_{D3}>I_{D2}$	$P_{\mathrm{con}\_D3}>P_{\mathrm{con}\_D2}$

4) *D_2 and D_3:* The D_3 takes more current in comparison with D_2, and $I_{D3} > I_{D2}$, which causes $P_{\mathrm{con}\_D3} > P_{\mathrm{con}\_D2}$ according to (2).

V. Proposed Power Loss Balancing Control for FBSMs

A. Analysis of Current Difference Integral

The current differences Δi_{T14} between T_1 and T_4, Δi_{D14} between D_1 and D_4, Δi_{T32} between T_3 and T_2, and Δi_{D32} between D_3 and D_2 are

$$\begin{cases} \Delta i_{T14} = i_{T1} - i_{T4} \\ \Delta i_{D14} = i_{D1} - i_{D4} \\ \Delta i_{T32} = i_{T3} - i_{T2} \\ \Delta i_{D32} = i_{D3} - i_{D2}. \end{cases} \tag{14}$$

The current difference integrals ΔI_{T14}, ΔI_{D14}, ΔI_{T32}, and ΔI_{D32} are

$$\begin{cases} \Delta I_{T14} = \int_0^t \Delta i_{T14} dt \\ \Delta I_{D14} = \int_0^t \Delta i_{D14} dt \\ \Delta I_{T32} = \int_0^t \Delta i_{T32} dt \\ \Delta I_{D32} = \int_0^t \Delta i_{D32} dt. \end{cases} \tag{15}$$

According to Figs. 2 and 11, the semiconductor currents in the FBSM have the relationship as

$$\begin{cases} i_{T1} = i_{T4}, i_{D1} = i_{D4}, i_{T3} = i_{T2}, i_{D3} = i_{D2} (S_i = \pm 1) \\ i_{T1} = i_{D3}, i_{D1} = i_{T3}, i_{T4} = i_{D2}, i_{D4} = i_{T2} (S_i = 0). \end{cases} \tag{16}$$

Substituting (14) and (15) into (16), there is

$$\begin{cases} \Delta I_{T14} = \Delta I_{D32} \\ \Delta I_{T32} = \Delta I_{D14}. \end{cases} \tag{17}$$

The conduction loss differences $\Delta P_{\mathrm{con}\_T14}$ between T_1 and T_4, $\Delta P_{\mathrm{con}\_D14}$ between D_1 and D_4, $\Delta P_{\mathrm{con}\_T32}$ between T_3 and T_2, and $\Delta P_{\mathrm{con}\_D32}$ between D_3 and D_2 can be expressed as

$$\begin{cases} \Delta P_{\mathrm{con}\_T14} = P_{\mathrm{con}\_T1} - P_{\mathrm{con}\_T4} \\ \Delta P_{\mathrm{con}\_D14} = P_{\mathrm{con}\_D1} - P_{\mathrm{con}\_D4} \\ \Delta P_{\mathrm{con}\_T32} = P_{\mathrm{con}\_T3} - P_{\mathrm{con}\_T2} \\ \Delta P_{\mathrm{con}\_D32} = P_{\mathrm{con}\_D3} - P_{\mathrm{con}\_D2}. \end{cases} \tag{18}$$

Substituting (2) and (17) into (18), the relationship between current difference integrals and conduction loss differences can

TABLE V
RELATIONSHIP BETWEEN BM, ΔI_{T} (ΔI_{D}), AND $\Delta P_{\mathrm{CON\_T}}$ ($\Delta P_{\mathrm{CON\_D}}$)

BM	ΔI_{T14} (ΔI_{D32})	ΔI_{T32} (ΔI_{D14})	ΔP_{con_T14} (ΔP_{con_D32})	ΔP_{con_T32} (ΔP_{con_D14})
Mode 0A	↓	↓	↓	↓
Mode 0B	↑	↑	↑	↑

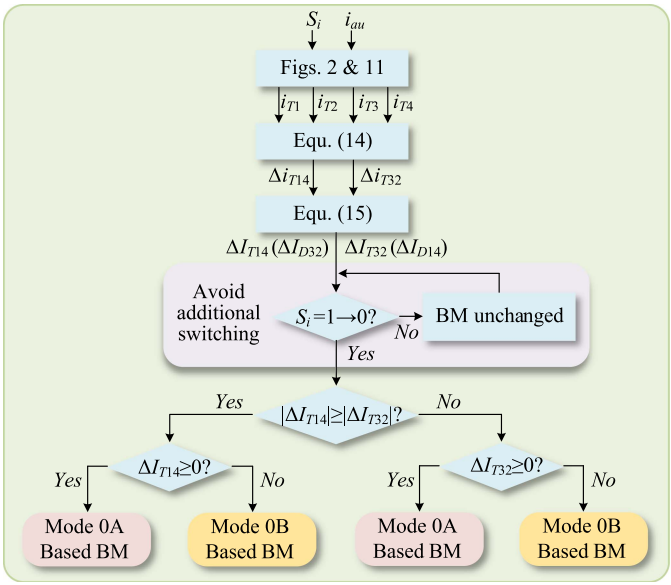

Fig. 12. Diagram of proposed CIC-PLBC for the ith FBSM.

be expressed as

$$\begin{cases} \Delta P_{\mathrm{con\_}T14} = (V_{T\mathrm{con}}/T_f)\cdot\Delta I_{T14} \\ \Delta P_{\mathrm{con\_}D14} = (V_{D\mathrm{con}}/T_f)\cdot\Delta I_{D14} \\ \Delta P_{\mathrm{con\_}T32} = (V_{T\mathrm{con}}/T_f)\cdot\Delta I_{T32} \\ \Delta P_{\mathrm{con\_}D32} = (V_{D\mathrm{con}}/T_f)\cdot\Delta I_{D32} \end{cases} \tag{19}$$

with

$$\begin{cases} \Delta P_{\mathrm{con\_}T14} = (V_{T\mathrm{con}}/V_{D\mathrm{con}})\cdot\Delta P_{\mathrm{con\_}D32} \\ \Delta P_{\mathrm{con\_}T32} = (V_{T\mathrm{con}}/V_{D\mathrm{con}})\cdot\Delta P_{\mathrm{con\_}D14}. \end{cases} \tag{20}$$

According to (17), (19), (20), and Tables III and IV, the relationship between selected BM and current difference integral, conduction loss difference can be obtained, as given in Table V, as follows.

1) *Mode 0A:* The ΔI_{T14}, ΔI_{D32}, ΔI_{T32}, and ΔI_{D14} would be reduced, which results in that the conduction loss differences $\Delta P_{\mathrm{con\_}T14}$, $\Delta P_{\mathrm{con\_}D32}$, $\Delta P_{\mathrm{con\_}T32}$, and $\Delta P_{\mathrm{con\_}D14}$ would be reduced.
2) *Mode 0B:* The ΔI_{T14}, ΔI_{D32}, ΔI_{T32}, and ΔI_{D14} would be increased, which results in that the conduction loss differences $\Delta P_{\mathrm{con\_}T14}$, $\Delta P_{\mathrm{con\_}D32}$, $\Delta P_{\mathrm{con\_}T32}$, and $\Delta P_{\mathrm{con\_}D14}$ would be increased.

B. Proposed Power Loss Balancing Control

Based on above analysis, a CIC-PLBC for the ith FBSM is proposed, as shown in Fig. 12, which can make $\Delta P_{\mathrm{con\_}T14}$, $\Delta P_{\mathrm{con\_}D14}$, $\Delta P_{\mathrm{con\_}T32}$, and $\Delta P_{\mathrm{con\_}D32}$ close to 0 through selecting Mode 0A or Mode 0B for BM, so as to make T_1's loss close to T_4's loss, T_2's loss close to T_3's loss, D_1's loss close to D_4's loss, and D_2's loss close to D_3's loss, and accordingly improve the power loss distribution in the FBSM.

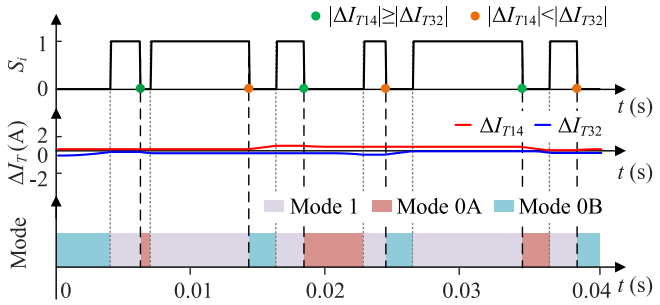

Fig. 13. Diagram of BM selection with proposed CIC-PLBC.

In Fig. 12, based on the switching function S_i, the arm current i_{au}, and Figs. 2 and 11, the currents i_{T1}–i_{T4} of switches T_1–T_4 can be obtained. Then, the current differences Δi_{T14} and Δi_{T32} can be obtained based on (14). Afterward, the current difference integrals ΔI_{T14} (ΔI_{D32}) and ΔI_{T32} (ΔI_{D14}) can be obtained based on (15). At the moment when S_i is switched from 1 to 0, the Mode 0A or Mode 0B are selected for BM based on ΔI_{T14} and ΔI_{T32}, so as to balance the power losses in the FBSM, as follows.

1) *If* $|\Delta I_{T14}| \geq |\Delta I_{T32}|$ *and* $\Delta I_{T14} \geq 0$: $|\Delta P_{\mathrm{con\_}T14}| \geq |\Delta P_{\mathrm{con\_}T32}|$, $|\Delta P_{\mathrm{con\_}D32}| \geq |\Delta P_{\mathrm{con\_}D14}|$, $\Delta P_{\mathrm{con\_}T14} \geq 0$, and $\Delta P_{\mathrm{con\_}D32} \geq 0$ based on (19) and (20). According to Table V, Mode 0A should be selected for BM. As a result, the ΔI_{T14} will be reduced, which reduces $\Delta P_{\mathrm{con\_}T14}$ and $\Delta P_{\mathrm{con\_}D32}$.
2) *If* $|\Delta I_{T14}| \geq |\Delta I_{T32}|$ *and* $\Delta I_{T14} < 0$: $|\Delta P_{\mathrm{con\_}T14}| \geq |\Delta P_{\mathrm{con\_}T32}|$, $|\Delta P_{\mathrm{con\_}D32}| \geq |\Delta P_{\mathrm{con\_}D14}|$, $\Delta P_{\mathrm{con\_}T14} < 0$, and $\Delta P_{\mathrm{con\_}D32} < 0$ based on (19) and (20). According to Table V, Mode 0B should be selected for BM. As a result, the ΔI_{T14} will be increased, which increases $\Delta P_{\mathrm{con\_}T14}$ and $\Delta P_{\mathrm{con\_}D32}$.
3) *If* $|\Delta I_{T14}| < |\Delta I_{T32}|$ *and* $\Delta I_{T32} \geq 0$: $|\Delta P_{\mathrm{con\_}T14}| < |\Delta P_{\mathrm{con\_}T32}|$, $|\Delta P_{\mathrm{con\_}D32}| < |\Delta P_{\mathrm{con\_}D14}|$, $\Delta P_{\mathrm{con\_}T32} \geq 0$, and $\Delta P_{\mathrm{con\_}D14} \geq 0$ based on (19) and (20). According to Table V, Mode 0A should be selected for BM. As a result, the ΔI_{T32} will be reduced, which reduces $\Delta P_{\mathrm{con\_}T32}$ and $\Delta P_{\mathrm{con\_}D14}$.
4) *If* $|\Delta I_{T14}| < |\Delta I_{T32}|$ *and* $\Delta I_{T32} < 0$: $|\Delta P_{\mathrm{con\_}T14}| < |\Delta P_{\mathrm{con\_}T32}|$, $|\Delta P_{\mathrm{con\_}D32}| < |\Delta P_{\mathrm{con\_}D14}|$, $\Delta P_{\mathrm{con\_}T32} < 0$, and $\Delta P_{\mathrm{con\_}D14} < 0$ based on (19) and (20). According to Table V, Mode 0B should be selected for BM. As a result, the ΔI_{T32} will be increased, which increases $\Delta P_{\mathrm{con\_}T32}$ and $\Delta P_{\mathrm{con\_}D14}$.

To avoid introducing additional switching loss, if the S_i is unchanged or switched from 0 to 1 during two adjacent control cycles, the selected BM should be kept invariable, as shown in Fig. 12. Fig. 13 shows an example of the BM selection. With the proposed CIC-PLBC, the conduction loss differences $\Delta P_{\mathrm{con\_}T14}$, $\Delta P_{\mathrm{con\_}T32}$, $\Delta P_{\mathrm{con\_}D14}$, and $\Delta P_{\mathrm{con\_}D32}$ would be

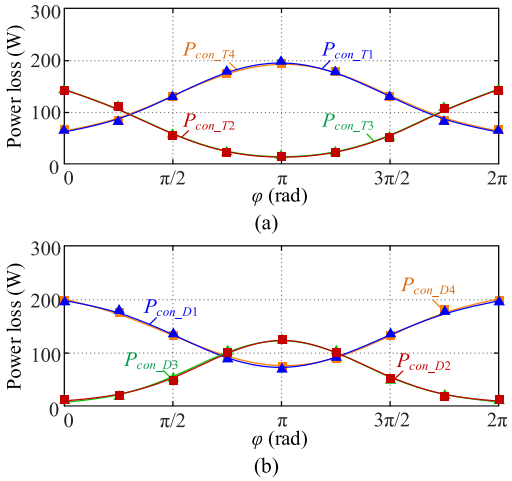

Fig. 14. Conduction losses with proposed CIC-PLBC. (a) Conduction losses of T_1–T_4. (b) Conduction losses of D_1–D_4.

TABLE VI
SYSTEM PARAMETERS FOR SIMULATION

Parameter	Value
Rated power	10 MVA
DC link voltage V_{dc}	20 kV
Grid frequency	50 Hz
Transformer leakage reactance	10%
Number of FBSM per arm N	20
Rated SM capacitance C	10 mF
Arm inductance L_s	5 mH
Filter inductance L_f	3 mH
Semiconductor	FZ1200R17HP4

controlled close to 0. Since the switching loss of the MMC with numerous SMs is quite small and it has little effect on power loss unbalancing [10], as shown in Figs. 3–10, the proposed CIC-PLBC can effectively balance the power losses in the FBSM.

C. Conduction Loss Analysis of FBSM

Fig. 14 shows the conduction losses of semiconductors in the FBSM of MMC working at rated apparent power listed in Table VI and $m = 0.8$, which is derived from the simulation system in Section VI. Here, the proposed CIC-PLBC method is adopted. Compared with Figs. 3–10, where the FBSM works with only Mode 0A-based BM, the proposed CIC-PLBC can not only effectively balance conduction losses in the FBSM, but also reduce the maximum conduction loss among semiconductors.

D. Switching Loss Analysis of FBSM

Fig. 15 shows the switching losses in the FBSM of MMC working at rated apparent power and $\varphi = 0$. In Fig. 15, $m = 0.8$ and the FBSM works with only Mode 0A-based BM, only Mode 0B-based BM, and proposed CIC-PLBC, respectively. From Fig. 15, the switching loss distribution in the FBSM is also improved with proposed CIC-PLBC. In addition, the proposed

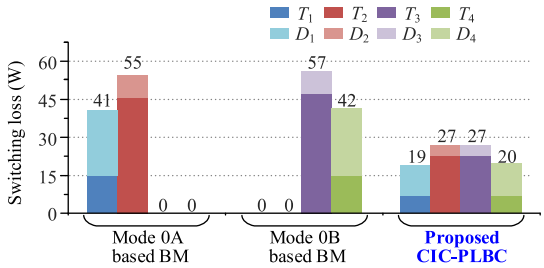

Fig. 15. Switching losses of the FBSM with only mode 0A-based BM, only mode 0B-based BM, and proposed CIC-PLBC.

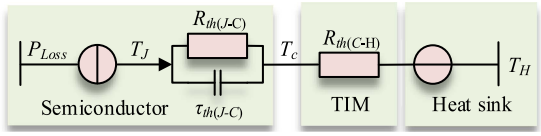

Fig. 16. Thermal network of the semiconductor.

CIC-PLBC does not introduce additional switching loss, where the total switching loss of the FBSM is 93 W with proposed CIC-PLBC, which is close to 96 W with only Mode 0A-based BM and 99 W with only Mode 0B-based BM.

E. Temperature Fluctuation Analysis

Fig. 16 shows the equivalent thermal network of the semiconductor, where $R_{\mathrm{th}(J\text{-}C)}$ is the thermal resistance from junction to case, $R_{\mathrm{th}(C\text{-}H)}$ is the thermal resistance of thermal interface material (TIM) from case to heat sink, and $\tau_{\mathrm{th}(J\text{-}C)}$ is the thermal time constant from junction to case [20], [21]. T_J, T_c, and T_H are the temperature of junction, case, and heat sink, respectively. To simplify the analysis, the T_H is considered as a constant value 50 °C [22]. Based on this model, the junction temperature of semiconductors in the FBSM can be obtained.

Fig. 17 shows the junction temperatures of the switches T_1–T_4 and diodes D_1–D_4 in the FBSM of MMC working at rated apparent power listed in Table VI and $\varphi = 0$, which is derived from the simulation system in Section VI. Here, the proposed CIC-PLBC is enabled at 2.2 s. Before 2.2 s, the control in [16] is adopted, where the Mode 0A and Mode 0B are selected in rotation for BM, and the rotation cycle is one fundamental cycle. Compared with control in [16], both the junction temperature fluctuations and the maximum temperature of semiconductors are effectively reduced with proposed CIC-PLBC, as shown in Fig. 17. It can be observed that T_1's temperature fluctuation is reduced from 2.09 to 1.35 °C, with a 35.4% reduction, and its maximum temperature is reduced from 56.76 to 56.38 °C, with a 0.7% reduction. Similarly, the temperature fluctuation and the maximum temperature of T_2 are reduced by 64.2% and 3.5%, respectively; those of T_3 are reduced by 63.7% and 3.4%; those of T_4 are reduced by 35.7% and 0.8%; those of D_1 are reduced by 21.5% and 0.9%; those of D_2 are reduced by 51.7% and 1.3%; those of D_3 are reduced by 51.2% and 1.3%; those of D_4 are reduced by 21.5% and 0.7%, respectively.

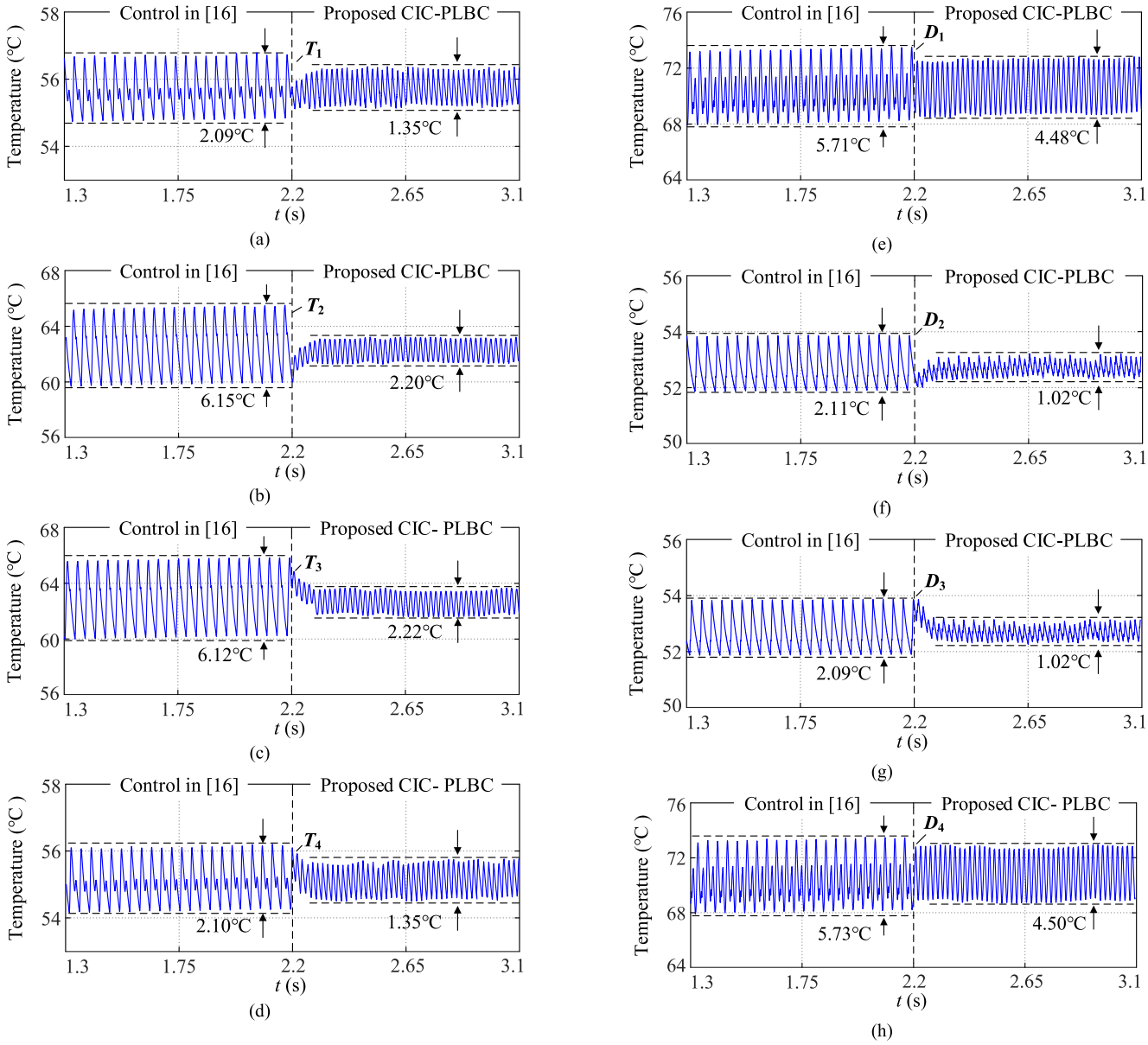

Fig. 17. Junction temperatures with control in [16] and proposed CIC-PLBC. (a) T_1. (b) T_2. (c) T_3. (d) T_4. (e) D_1. (f) D_2. (g) D_3. (h) D_4.

F. Reliability Analysis

The number of power cycles to failure N_f of the semiconductor is [23]

$$N_f = A(\Delta T)^{\beta_1} \cdot \exp\left(\frac{\beta_2}{T_{\max}+273}\right) \cdot \left(\frac{t_{\text{test}}}{1.5}\right)^{\beta_3} \tag{21}$$

where A, β_1, β_2, and β_3 are fitting parameters. $A = 1.42 \times 10^{12}$, $\beta_1 = -7.14$, $\beta_2 = 5154$, and $\beta_3 = -0.3$, and t_{test} ranges from 0.1 to 60 s. ΔT is the junction temperature fluctuation, and $T_{\max}$ is the maximum junction temperature.

The consumed lifetime per year of the semiconductor is [21]

$$C_L = \frac{365 \times 24 \times 3600 \times 50}{N_f}. \tag{22}$$

The reliability function $R_{com}(t)$ of the semiconductor can be expressed as [24], [25]

$$R_{com}(t) = e^{-C_L t}. \tag{23}$$

According to the reliability block diagram [23], the failure function $F_{\text{MMC}}(t)$ of the MMC can be expressed by semiconductors' reliability functions $R_{com}(t)$, as

$$F_{\text{MMC}}(t) = 1 - \prod_{k=1}^{6}\left[\prod_{i=1}^{N}\left[\prod_{j=1}^{8} R_{comkij}(t)\right]\right]. \tag{24}$$

Based on above analysis, the lifetime of the MMC can be obtained, as shown in Fig. 18. Here, the control in [16] and proposed CIC-PLBC are adopted, respectively. In Fig. 18, the MMC's lifetime with proposed CIC-PLBC is set as the base

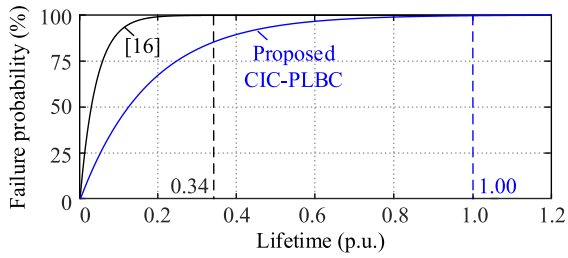

Fig. 18. Failure probability of MMC with control in [16] and CIC-PLBC.

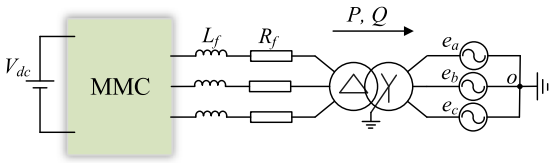

Fig. 19. Block diagram of the MMC simulation system.

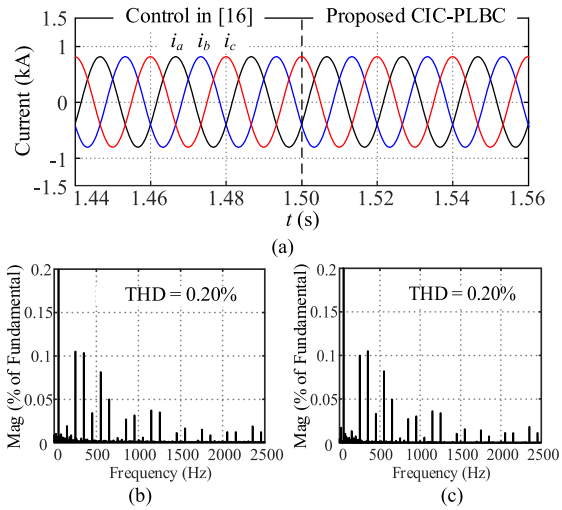

Fig. 20. (a) i_a, i_b, and i_c. (b) Harmonic spectrum of i_a with control in [16]. (c) Harmonic spectrum of i_a with proposed CIC-PLBC.

value. Due to the reduced temperature fluctuation and the maximum temperature, as shown in Fig. 17, the proposed CIC-PLBC has significant effects on the improvement of the MMC's lifetime. Compared with the control in [16], the lifetime of MMC with proposed CIC-PLBC is improved from 0.34 to 1 per unit, with a 194.1% increase.

VI. Simulation Studies

To verify the effectiveness of proposed CIC-PLBC, the simulation studies of the three-phase MMC system are performed with the time-domain simulation tool PSCAD/EMTDC, as shown in Fig. 19. The main simulation parameters are listed in Table VI.

A. MMCs Working at $m = 0.8$ and $\varphi = 0$

Fig. 20(a) shows the grid currents i_a, i_b, and i_c of MMC working at $m = 0.8$ and $\varphi = 0$. Here, the proposed CIC-PLBC is

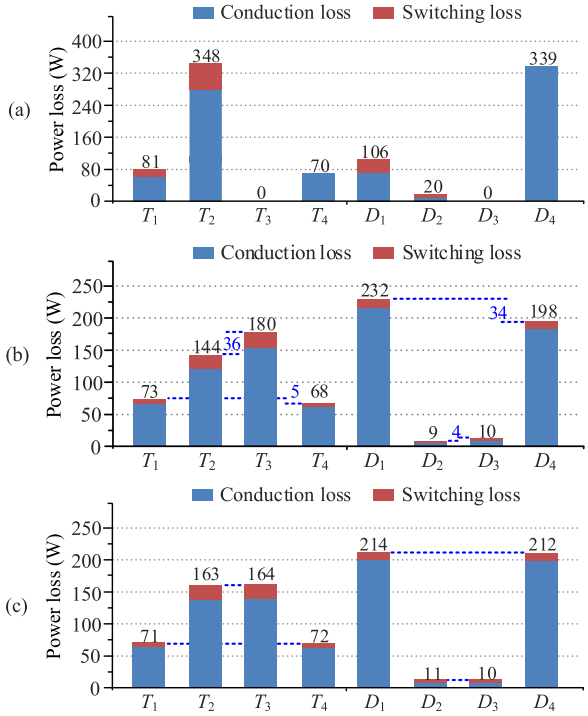

Fig. 21. Power loss distribution when $m = 0.8$ and $\varphi = 0$. (a) With only mode 0A-based BM. (b) With control in [16]. (c) With proposed CIC-PLBC.

enabled at 1.5 s. Before 1.5 s, the FBSM works with control in [16]. Fig. 20(b) and (c) shows the spectrum of i_a with control in [16] and proposed CIC-PLBC, respectively. It can be observed that the proposed CIC-PLBC has little impact on the output current of the MMC.

Fig. 21(a)–(c) shows the power loss distribution in the FBSM of MMC working at $m = 0.8$ and $\varphi = 0$, where the FBSM works with only Mode 0A-based BM, the control in [16], and proposed CIC-PLBC, respectively. From Fig. 21(a), the power losses in the FBSM with only Mode 0A-based BM is extremely unbalanced. From Fig. 21(b), the power losses between T_1 and T_4, T_2 and T_3, D_1 and D_4, and D_2 and D_3 are still unbalanced with the control in [16]. Compared with Fig. 21(a) and (b), the proposed CIC-PLBC can effectively improve the power loss distribution in the FBSM, as shown in Fig. 21(c).

B. MMCs Working at $m = 0.8$ and $\varphi = \pi/2$

Fig. 22(a) and (b) shows the power loss distribution in the FBSM of MMC working at $m = 0.8$ and $\varphi = \pi/2$, where the FBSM works with the control in [16] and proposed CIC-PLBC, respectively. Compared with Fig. 22(a), Fig. 22(b) shows that the proposed CIC-PLBC can effectively improve the power loss distribution in the FBSM.

C. MMCs Working at $m = 0.8$ and $\varphi = \pi$

Fig. 23(a) and (b) shows the power loss distribution in the FBSM of MMC working at $m = 0.8$ and $\varphi = \pi$, where the FBSM works with the control in [16] and proposed CIC-PLBC, respectively. Compared with Figs. 23(a) and (b) shows that the

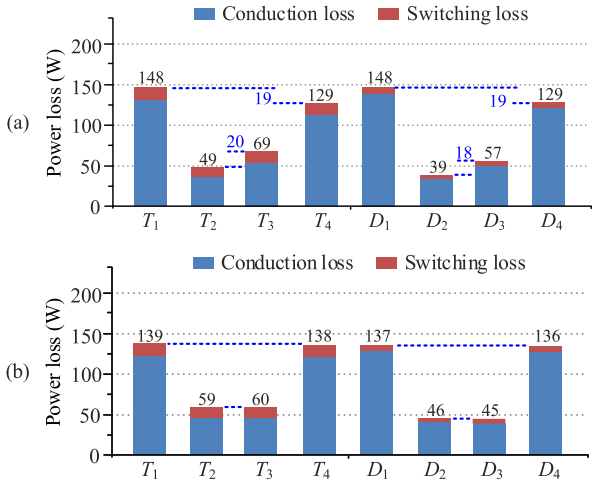

Fig. 22. Power loss distribution when $m = 0.8$ and $\varphi = \pi/2$. (a) With control in [16]. (b) With proposed CIC-PLBC.

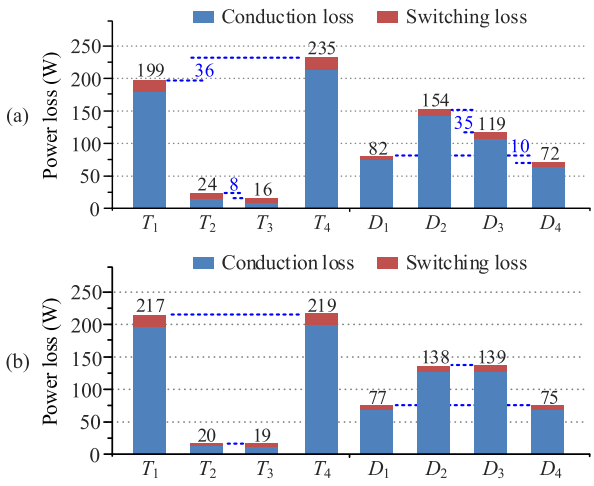

Fig. 23. Power loss distribution when $m = 0.8$ and $\varphi = \pi$. (a) With control in [16]. (b) With proposed CIC-PLBC.

proposed CIC-PLBC can effectively improve the power loss distribution in the FBSM.

D. MMCs Working at $m = 0.8$ and $\varphi = 3\pi/2$

Fig. 24(a) and (b) shows the power loss distribution in the FBSM of MMC working at $m = 0.8$ and $\varphi = 3\pi/2$, where the FBSM works with the control in [16] and proposed CIC-PLBC, respectively. Compared with Fig. 24(a), Fig. 24(b) shows that the proposed CIC-PLBC can effectively improve the power loss distribution in the FBSM.

E. MMCs Working at $m = 1.5$ and $\varphi = 0$

Fig. 25(a) and (b) shows the power loss distribution in the FBSM of MMC working at $m = 1.5$ and $\varphi = 0$, where the FBSM works with the control in [16] and proposed CIC-PLBC, respectively. Compared with Fig. 25(a), Fig. 25(b) shows that the proposed CIC-PLBC can also effectively improve the power loss distribution in the FBSM when the MMC works with overmodulation.

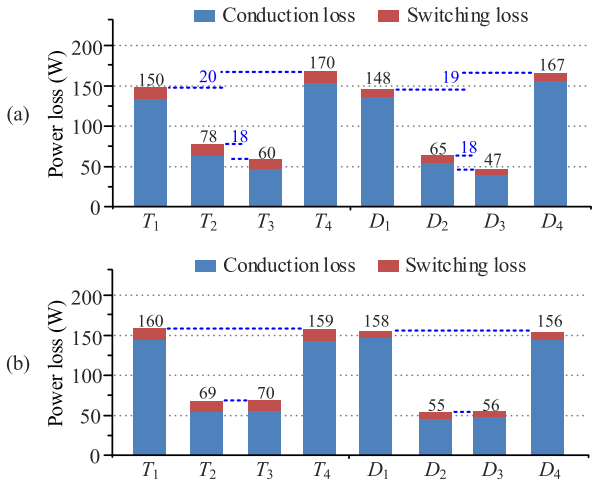

Fig. 24. Power loss distribution when m = 0.8 and $\varphi = 3\pi/2$. (a) With control in [16]. (b) With proposed CIC-PLBC.

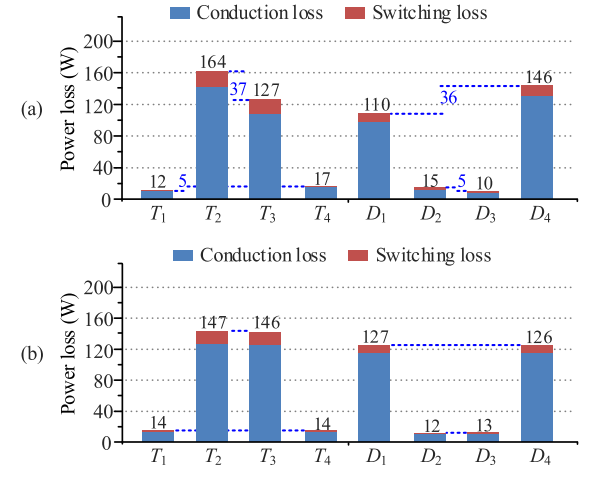

Fig. 25. Power loss distribution when $m = 1.5$ and $\varphi = 0$. (a) With control in [16]. (b) With proposed CIC-PLBC.

VII. Experimental Studies

A three-phase MMC is built in the laboratory to verify the proposed CIC-PLBC method, as shown in Fig. 26(a) and (b). The dc-side voltage of the MMC is supported by a dc source SGA600/10 paralleled with a resistor, and the ac-side of the MMC is connected to the grid via an autotransformer (AT). The system parameters are listed in Table VII.

A. MMCs Working at $\varphi = 0$

Fig. 27 shows the power loss distribution in the FBSM of MMC working at the rated apparent power and $\varphi = 0$. Before enabling the proposed CIC-PLBC, the FBSM works with control in [16]. Fig. 27(a) shows the loss energy differences ΔE_{T14} between T_1 and T_4, ΔE_{T23} between T_2 and T_3, ΔE_{D14} between D_1 and D_4, and ΔE_{D23} between D_2 and D_3, respectively. The

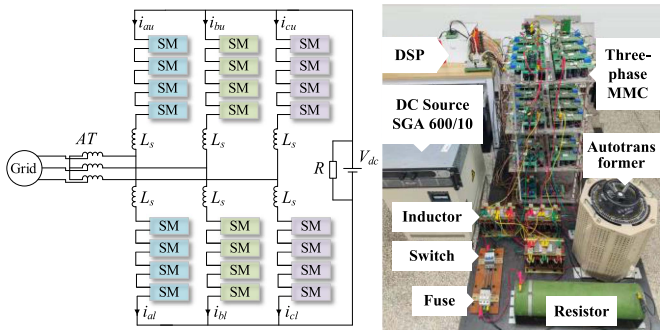

(a) (b)

Fig. 26. (a) Block diagram of experimental circuit. (b) Experimental platform.

TABLE VII
EXPERIMENTAL SYSTEM PARAMETERS

Parameter	Value
Rated Power (kW)	1
DC-link voltage V_{dc} (V)	200
RMS value of line-to-line (V)	100
Rated frequency (Hz)	50
Number of SM per arm N	4
SM capacitance (mF)	2.35
Arm inductance L_s (mH)	3
Filter inductance L_f(mH)	3

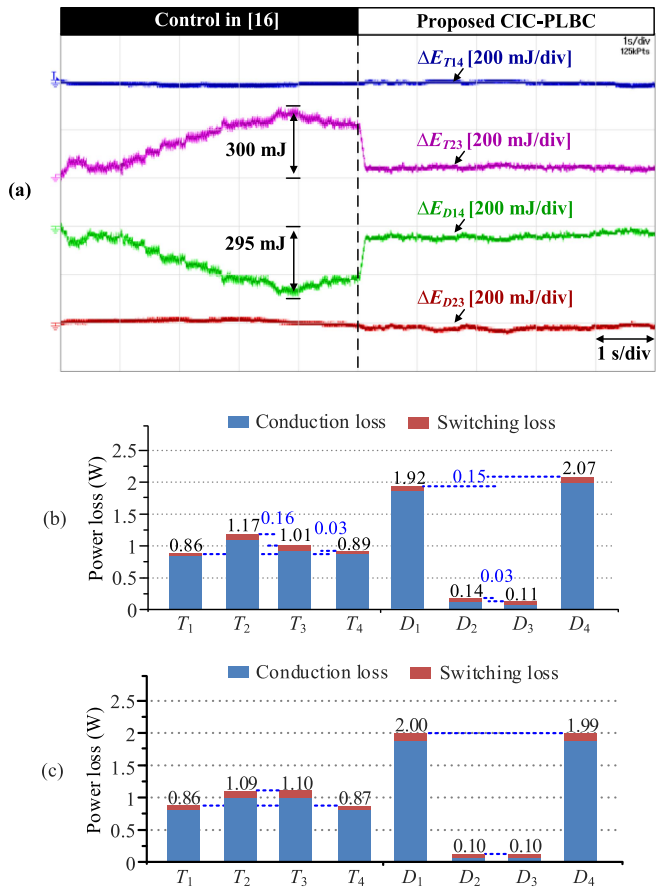

Fig. 27. (a) Loss energy differences ΔE_{T14}, ΔE_{T23}, ΔE_{D14}, and ΔE_{D23} when $\varphi = 0$. (b) Power loss distribution with control in [16]. (c) Power loss distribution with proposed CIC-PLBC.

loss energy differences are

$$\begin{cases} \Delta E_{T14} = \int_0^t (P_{\text{Loss\_}T1} - P_{\text{Loss\_}T4})dt \\ \Delta E_{T23} = \int_0^t (P_{\text{Loss\_}T2} - P_{\text{Loss\_}T3})dt \\ \Delta E_{D14} = \int_0^t (P_{\text{Loss\_}D1} - P_{\text{Loss\_}D4})dt \\ \Delta E_{D23} = \int_0^t (P_{\text{Loss\_}D2} - P_{\text{Loss\_}D3})dt. \end{cases} \tag{25}$$

From (25), taking ΔE_{T14} as an example, if ΔE_{T14} increases, the power losses between T_1 and T_4 are unbalanced and $P_{\text{Loss\_}T1} > P_{\text{Loss\_}T4}$; if ΔE_{T14} decreases, the power losses between T_1 and T_4 are unbalanced and $P_{\text{Loss\_}T1} < P_{\text{Loss\_}T4}$; if ΔE_{T14} remain unchanged, the power losses between T_1 and T_4 are balanced and $P_{\text{Loss\_}T1} = P_{\text{Loss\_}T4}$. Fig. 27(b) and (c) shows the power loss distribution in the FBSM with control in [16] and proposed CIC-PLBC, respectively.

From Fig. 27(a), the loss energy differences ΔE_{T23} and ΔE_{D14} change drastically with the control in [16], which indicates that the power losses between T_2 and T_3, and D_1 and D_4 are unbalanced, as shown in Fig. 27(b).

After the proposed CIC-PLBC is enabled, the loss energy differences ΔE_{T14}, ΔE_{T23}, ΔE_{D14}, and ΔE_{D23} are almost unchanged, which indicates that the power losses of T_1 and T_4, T_2 and T_3, D_1 and D_4, and D_2 and D_3 are close to each other, as shown in Fig. 27(c).

B. MMCs Working at $\varphi = \pi/2$

Fig. 28 shows the power loss distribution in the FBSM of MMC working at rated apparent power and $\varphi = \pi/2$. Before enabling the proposed CIC-PLBC, the FBSM works with the control in [16]. Fig. 28(a) shows the loss energy differences ΔE_{T14}, ΔE_{T23}, ΔE_{D14}, and ΔE_{D23}. Fig. 28(b) and (c) shows the power loss distribution in the FBSM with control in [16] and proposed CIC-PLBC, respectively.

From Fig. 28(a), the loss energy differences ΔE_{T23} and ΔE_{D14} change drastically with the control in [16], which indicates that the power losses between T_2 and T_3, and D_1 and D_4 are unbalanced, as shown in Fig. 28(b).

After the proposed CIC-PLBC is enabled, the loss energy differences ΔE_{T14}, ΔE_{T23}, ΔE_{D14}, and ΔE_{D23} are almost unchanged, which indicates that the power losses of T_1 and T_4, T_2 and T_3, D_1 and D_4, and D_2 and D_3 are close to each other, as shown in Fig. 28(c).

C. MMCs Working at $\varphi = \pi$

Fig. 29 shows the power loss distribution in the FBSM of MMC working at rated apparent power and $\varphi = \pi$. Before enabling the proposed CIC-PLBC, the FBSM works with control in [16]. Fig. 29(a) shows the loss energy differences ΔE_{T14}, ΔE_{T23}, ΔE_{D14}, and ΔE_{D23}. Fig. 29(b) and (c) shows the power loss distribution in the FBSM with control in [16] and proposed CIC-PLBC, respectively.

From Fig. 29(a), the loss energy differences ΔE_{T14} and ΔE_{D23} change drastically with the control in [16], which indicates that the power losses between T_1 and T_4, and D_2 and

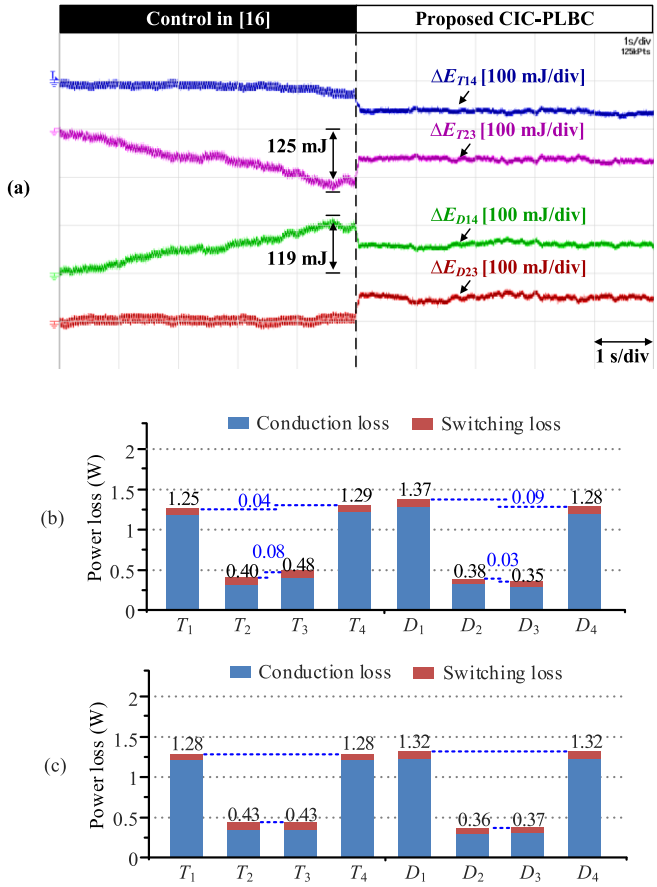

Fig. 28. (a) Loss energy differences when $\varphi = \pi/2$. (b) Power loss distribution with control in [16]. (c) Power loss distribution with proposed CIC-PLBC.

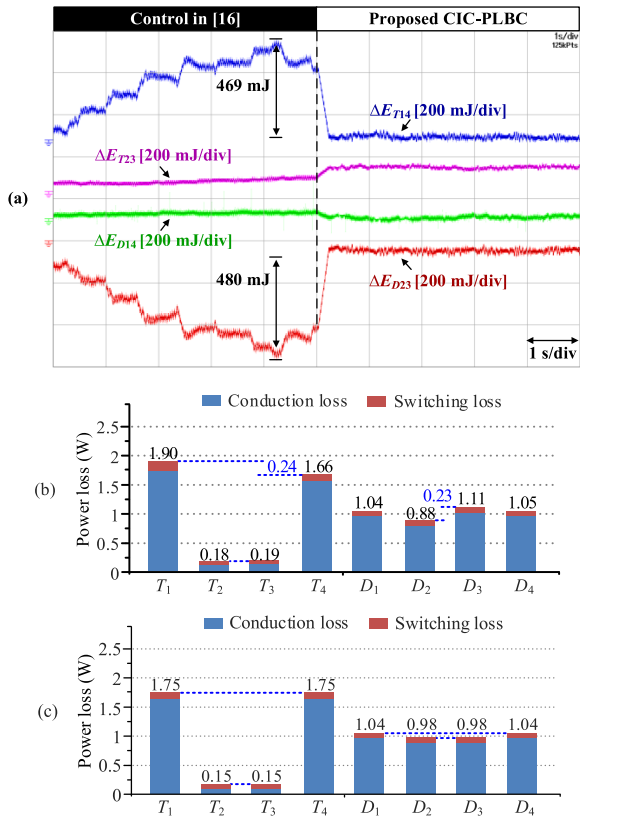

Fig. 29. (a) Loss energy differences when $\varphi = \pi$. (b) Power loss distribution with control in [16]. (c) Power loss distribution with proposed CIC-PLBC.

D_3 are unbalanced, as shown in Fig. 29(b). After the proposed CIC-PLBC method is enabled, the loss energy differences ΔE_{T14}, ΔE_{T23}, ΔE_{D14}, and ΔE_{D23} are almost unchanged, which indicates that the power losses of T_1 and T_4, T_2 and T_3, D_1 and D_4, and D_2 and D_3 are close to each other, respectively, as shown in Fig. 29(c).

D. MMCs Working at $\varphi = 3\pi/2$

Fig. 30 shows the power loss distribution in the FBSM of MMC working at rated apparent power and $\varphi = 3\pi/2$. Before enabling the proposed CIC-PLBC, the FBSM works with control in [16]. Fig. 30(a) shows the loss energy differences ΔE_{T14}, ΔE_{T23}, ΔE_{D14}, and ΔE_{D23}. Fig. 30(b) and (c) shows the power loss distribution in the FBSM with control in [16] and proposed CIC-PLBC, respectively.

From Fig. 30(a), the loss energy differences ΔE_{T23} and ΔE_{D14} change drastically with the control in [16], which indicates that the power losses between T_2 and T_3, and D_1 and D_4 are unbalanced, as shown in Fig. 30(b). After the proposed CIC-PLBC is enabled, the loss energy differences ΔE_{T14}, ΔE_{T23}, ΔE_{D14}, and ΔE_{D23} are almost unchanged, which indicates that the power losses of T_1 and T_4, T_2 and T_3, D_1 and D_4, and D_2 and D_3 are close to each other, as shown in Fig. 30(c).

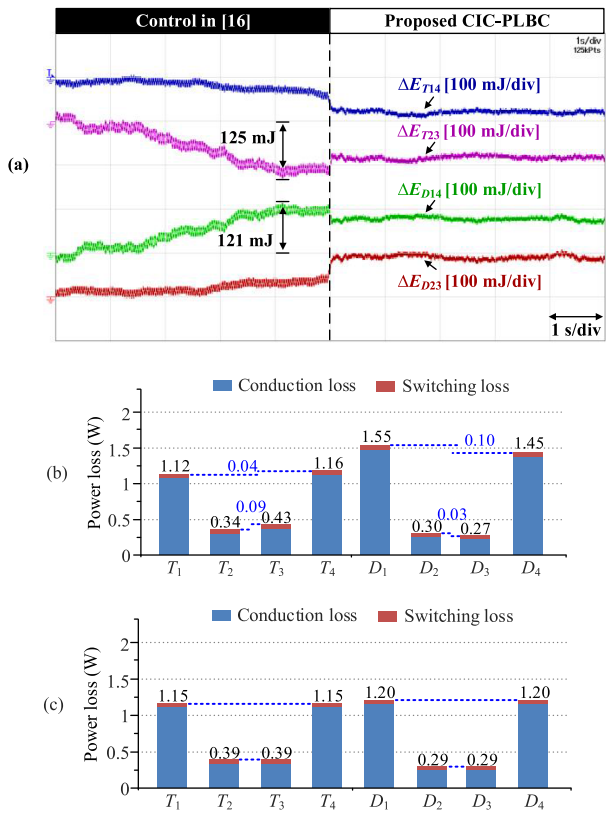

Fig. 30. (a) Loss energy differences when $\varphi = 3\pi/2$. (b) Power loss distribution with control in [16]. (c) Power loss distribution with proposed CIC-PLBC.

VIII. Conclusion

This article analyzed the power loss distribution of the semiconductors in the FBSM of the MMC in details. The uneven power loss distribution in the FBSM would affect the reliability of MMC. A current integral comparison-based power loss balancing control for the FBSM was proposed in this article, where two types of BMs of the FBSM can be selected by comparing the semiconductor current difference integral values in the FBSM. The proposed control can not only balance the power losses in the FBSM, but also reduce the temperature fluctuation of the semiconductors, which significantly improves the reliability of the MMC. Simulation and experimental results verify the proposed control.

References

[1] C. Liu, F. Deng, J. Zhang, X. Cai, Z. Chen, and F. Blaabjerg, "Power loss reduction control for modular multilevel converters based on resistor controllable submodule," *IEEE Trans. Power Electron.*, vol. 37, no. 8, pp. 9767–9776, Aug. 2022.

[2] F. Deng, C. Liu, Q. Wang, R. Zhu, X. Cai, and Z. Chen, "A currentless submodule individual voltage balancing control for modular multilevel converters," *IEEE Trans. Ind. Electron.*, vol. 67, no. 11, pp. 9370–9382, Nov. 2020.

[3] H. Li, F. Deng, J. Zhao, J. Tian, Y. Lu, and G. Li, "Variable sampling frequency-based SM power loss balancing control for MMCs with bypassed faulty SMs," *IEEE Trans. Power Electron.*, vol. 38, no. 7, pp. 9006–9018, Jul. 2023.

[4] F. Deng, Q. Yu, Q. Wang, R. Zhu, X. Cai, and Z. Chen, "Suppression of DC-link current ripple for modular multilevel converters under phase-disposition PWM," *IEEE Trans. Power Electron.*, vol. 35, no. 3, pp. 3310–3324, Mar. 2020.

[5] S. Wenig, M. Goertz, C. Hirsching, M. Suriyah, and T. Leibfried, "On full-bridge bipolar MMC-HVDC control and protection for transient fault and interaction studies," *IEEE Trans. Power Del.*, vol. 33, no. 6, pp. 2864–2873, Dec. 2018.

[6] F. Deng et al., "Protection scheme for modular multilevel converters under diode open-circuit faults," *IEEE Trans. Power Electron.*, vol. 33, no. 4, pp. 2866–2877, Apr. 2018.

[7] C. Zhao, Y. Li, Z. Li, P. Wang, X. Ma, and Y. Luo, "Optimized design of full-bridge modular multilevel converter with low energy storage requirements for HVdc transmission system," *IEEE Trans. Power Electron.*, vol. 33, no. 1, pp. 97–109, Jan. 2018.

[8] J. Hu, M. Xiang, L. Lin, M. Lu, J. Zhu, and Z. He, "Improved design and control of FBSM MMC with boosted AC voltage and reduced DC capacitance," *IEEE Trans. Ind. Electron.*, vol. 65, no. 3, pp. 1919–1930, Mar. 2018.

[9] F. Deng et al., "Power losses control for modular multilevel converters under capacitor deterioration," *IEEE J. Emerg. Sel. Topics Power Electron.*, vol. 8, no. 4, pp. 4318–4332, Dec. 2020.

[10] F. Hohmann and M. Bakran, "Improved performance for half-bridge cells with a parallel presspack diode," *IEEE Trans. Power Electron.*, vol. 34, no. 4, pp. 3091–3097, Apr. 2019.

[11] W. Li et al., "Thermal optimization of modular multilevel converters with surplus submodule active-bypass plus neutral-point-shift scheme under unbalanced grid conditions," *IEEE J. Emerg. Sel. Topics Power Electron.*, vol. 7, no. 3, pp. 1777–1788, Sep. 2019.

[12] M. M. C. Merlin and P. D. Mitcheson, "Active power losses distribution methods for the modular multilevel converter," in *Proc. IEEE 17th Workshop Control Model. Power Electron.*, 2016, pp. 1–6.

[13] J. Zhao, F. Deng, C. Liu, Q. Yu, Q. Wang, and J. Zhang, "Harmonic circulating current injection based power loss optimization control of bottom switch/diodes for modular multilevel converters," *CSEE J. Power Energy Syst.*, vol. 7, no. 6, pp. 1213–1226, Nov. 2021.

[14] H. Qiu, J. Wang, P. Tu, and Y. Tang, "Device-level loss balancing control for modular multilevel converters," *IEEE Trans. Power Electron.*, vol. 36, no. 4, pp. 4778–4790, Apr. 2021.

[15] J. Sheng et al., "Active thermal control for hybrid modular multilevel converter under overmodulation operation," *IEEE Trans. Power Electron.*, vol. 35, no. 4, pp. 4242–4255, Apr. 2020.

[16] K. Li, Z. Zhao, L. Yuan, S. Lu, and G. Feng, "An improved phase-shifted carrier-based modulation and loss distribution analysis for MMC using full-bridge sub-modules," in *Proc. IEEE 8th Int. Power Electron. Motion Control Conf.*, 2016, pp. 1252–1258.

[17] R. Zeng, L. Xu, L. Yao, and B. W. Williams, "Design and operation of a hybrid modular multilevel converter," *IEEE Trans. Power Electron.*, vol. 30, no. 3, pp. 1137–1146, Mar. 2015.

[18] S. Rohner, S. Bernet, M. Hiller, and R. Sommer, "Modulation, losses, and semiconductor requirements of modular multilevel converters," *IEEE Trans. Ind. Electron.*, vol. 57, no. 8, pp. 2633–2642, Aug. 2010.

[19] Infineon Technologies, "FZ1200R17HP4, datasheet," Infineon Technol., Neubiberg, Germany, [Online]. Available: https://www.alldatasheetcn.com/datasheet-pdf/pdf/397167/INFINEON/FZ1200R17HP4.html

[20] Y. Dong, H. Yang, W. Li, and X. He, "Neutral-point-shift-based active thermal control for a modular multilevel converter under a single-phase-to-ground fault," *IEEE Trans. Ind. Electron.*, vol. 66, no. 3, pp. 2474–2484, Mar. 2019.

[21] D. Zhou, F. Blaabjerg, T. Franke, M. Tønnes, and M. Lau, "Comparison of wind power converter reliability with low-speed and medium-speed permanent-magnet synchronous generators," *IEEE Trans. Ind. Electron.*, vol. 62, no. 10, pp. 6575–6584, Oct. 2015.

[22] F. Deng, J. Zhao, C. Liu, Z. Wang, X. Cai, and F. Blaabjerg, "Temperature-balancing control for modular multilevel converters under unbalanced grid voltages," *IEEE Trans. Power Electron.*, vol. 37, no. 4, pp. 4614–4625, Apr. 2022.

[23] Y. Zhang, H. Wang, Z. X. Wang, F. Blaabjerg, and M. Saeedifard, "Mission profile-based system-level reliability prediction method for modular multilevel converters," *IEEE Trans. Power Electron.*, vol. 35, no. 7, pp. 6916–6930, Jul. 2020.

[24] J. Guo, J. Liang, X. Zhang, P. D. Judge, X. Wang, and T. C. Green, "Reliability analysis of MMCs considering submodule designs with individual or series-operated IGBTs," *IEEE Trans. Power Del.*, vol. 32, no. 2, pp. 666–677, Apr. 2017.

[25] P. Tu, S. Yang, and P. Wang, "Reliability- and cost-based redundancy design for modular multilevel converter," *IEEE Trans. Power Electron.*, vol. 66, no. 3, pp. 2333–2342, Mar. 2019.

Huailong Li received the B.Eng. degree in electrical engineering from Jiangsu University, Zhenjiang, China, in 2021. He is currently working toward the Ph.D. degree in power electronics with the School of Electrical Engineering, Southeast University, Nanjing, China.

His main research interests include multilevel converters, high-voltage direct-current technology, and reliability of power devices.

Fujin Deng (Senior Member, IEEE) received the B.Eng. degree in electrical engineering from the China University of Mining and Technology, Jiangsu, China, in 2005, the M.Sc. degree in electrical engineering from Shanghai Jiao Tong University, Shanghai, China, in 2008, and the Ph.D. degree in energy technology from the Department of Energy Technology, Aalborg University, Aalborg, Denmark, in 2012.

In 2017, he joined the Southeast University and is currently a Professor with the School of Electrical Engineering, Southeast University, Nanjing, China. From 2013 to 2015 and from 2015 to 2017, he was a Postdoctoral Researcher and an Assistant Professor, respectively, with the Department of Energy Technology, Aalborg University, Aalborg, Denmark. His research interests include wind power generation, multilevel converters, HVdc technology, dc grids, and offshore wind farm-power systems dynamics.

Jie Tian was born in 1969 in Guizhou, China. He received the Ph.D. degree in electrical engineering from Zhejiang University, Hangzhou, China, in 1996.

In 2001, joined the NR Electric Company, Ltd., Nanjing, China, and is currently a Professor Engineer and Chief Expert of State Grid Corporation of China. His research interests include UHVdc, VSC-HVdc, and flexible ac transmission.

Yu Lu was born in Hubei, China, in 1979. He received the M.Sc. degree in electrical engineering from the Huazhong University of Science and Technology, Wuhan, China, in 2003.

In July 2003, he joined the NR Electric Company, Ltd., Nanjing, China, and is currently a Managing Director. His research interests include high-voltage direct current and UHVdc.

Gang Li was born in Henan, China, in 1983. He received the M.Sc. degree in electrical engineering from State Grid Electric Power Research Institute, Nanjing, China, in 2009.

He joined the NR Electric, Company, Ltd., in 2009 and is currently a Senior Engineer. His research interests include VSC-HVdc and flexible ac transmission.

Frede Blaabjerg (Fellow, IEEE) received the Ph.D. degree in electrical engineering from Aalborg University, Aalborg, Denmark, in 1995.

From 1987 to 1988, he was with ABB-Scandia, Randers, Denmark. He became an Assistant Professor in 1992, an Associate Professor in 1996, and a Full Professor of power electronics and drives in 1998. In 2017, he became a Villum Investigator. He is honoris causa with University Politehnica Timisoara (UPT), Timisoara, Romania, and Tallinn Technical University (TTU), Tallinn, Estonia. He has authored or coauthored more than 600 journal papers in the fields of power electronics and its applications, and is the coauthor of four monographs and editor of ten books in power electronics and its applications. His current research interests include power electronics and its applications, such as in wind turbines, PV systems, reliability, harmonics, and adjustable speed drives.

Dr. Blaabjerg was the recipient of the 32 IEEE Prize Paper Awards, IEEE PELS Distinguished Service Award in 2009, EPE-PEMC Council Award in 2010, IEEE William E. Newell Power Electronics Award 2014, Villum Kann Rasmussen Research Award 2014, Global Energy Prize in 2019, and 2020 IEEE Edison Medal. He was the Editor-in-Chief of the IEEE TRANSACTIONS ON POWER ELECTRONICS from 2006 to 2012. He has been a Distinguished Lecturer for the IEEE Power Electronics Society from 2005 to 2007 and for the IEEE Industry Applications Society from 2010 to 2011 as well as 2017 to 2018. In 2019–2020, he is the President of IEEE Power Electronics Society. He is the Vice-President of the Danish Academy of Technical Sciences too. He is nominated in 2014–2019 by Thomson Reuters to be between the most 250 cited researchers in engineering in the world.